

International Journal of Polymeric Materials and Polymeric Biomaterials



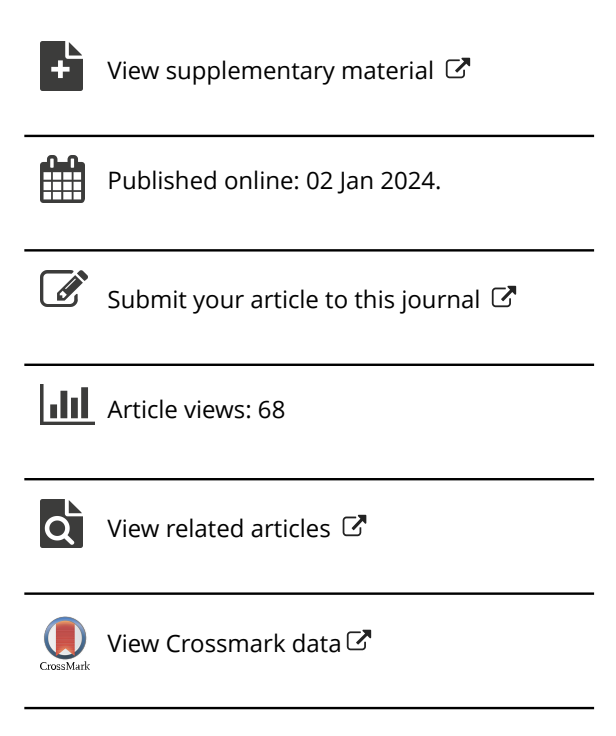
ISSN: (Print) (Online) Journal homepage: www.tandfonline.com/journals/gpom20

Graphene oxide-modified polythiophene nanohybrids: antibacterial properties and sonophotocatalytic degradation of dyes under visible-light irradiation

Shamella Myrick, Faith Nwanze, Audrey F Adcock, Xiuli Dong, Liju Yang & Ufana Riaz

To cite this article: Shamella Myrick, Faith Nwanze, Audrey F Adcock, Xiuli Dong, Liju Yang & Ufana Riaz (02 Jan 2024): Graphene oxide-modified polythiophene nanohybrids: antibacterial properties and sonophotocatalytic degradation of dyes under visible-light irradiation, International Journal of Polymeric Materials and Polymeric Biomaterials, DOI: 10.1080/00914037.2023.2299805

To link to this article: https://doi.org/10.1080/00914037.2023.2299805





RESEARCH ARTICLE



Check for updates

Graphene oxide-modified polythiophene nanohybrids: antibacterial properties and sonophotocatalytic degradation of dyes under visible-light irradiation

Shamella Myrick^a, Faith Nwanze^b, Audrey F Adcock^a, Xiuli Dong^c, Liju Yang^a and Ufana Riaz^b

^aDepartment of Pharmaceutical Sciences, Biomanufacturing Research Institute and Technology Enterprise (BRITE), North Carolina Central University, Durham, North Carolina, USA; ^bDepartment of Chemistry and Biochemistry, North Carolina Central University, Durham, North Carolina, USA; ^cDepartment of Microbiology and Immunology, School of Osteopathic Medicine, Campbell University, Buies Creek, North Carolina, USA

ABSTRACT

The present work highlights the synthesis of graphene oxide (GO) modified polythiophene (PTh) for its application as an antibacterial agent as well as a visible light active photocatalyst. PTh was synthesized via the interfacial polymerization method using FeCl₃ as initiator and then formulated as nanohybrids by mixing it in different weight ratios with graphene oxide (GO) i.e., 1 wt.%,3 wt.% and 5 wt. %. PTh and GO/PTh nanohybrids were characterized using FTIR, UV-visible, X-ray diffraction (XRD), X-ray photoelectron spectroscopy (XPS) and scanning electron microscopy (SEM) techniques. The polymerization of PTh as well as modification of PTh with GO was confirmed by IR studies, while the shifting of electronic transitions of PTH upon modification with GO were confirmed by the UV-visible studies. The degradation of dyes, Alizarin Yellow (AY), Basic Blue (BB) and Congo Red (CR) was carried out via sonophotocatalysis under visible light using PTh and GO/PTh as catalysts for a period of 60 min. The GO/PTh revealed higher degradation efficiency as compared to PTh. To evaluate its effectiveness as an antibacterial agent against Bacillus subtilis, disk diffusion inhibitory assay was carried out under dark and light conditions. The results showed that PTh and GO/PTh nanohybrids had bactericidal properties, regardless of light exposure. The results of the minimal inhibitory concentration (MIC) assay indicated the nanohybrid of 3-GO/PTh had the lowest MIC, followed by 1-GO/PTh and 5-GO/PTh.

ARTICLE HISTORY

Received 19 November 2023 Accepted 22 December 2023

KEYWORDS

Dye degradation; graphene oxide; polythiophene; sonophotocatalysis

1. Introduction

Conducting polymers (CPs) such as polyaniline (PANI)[1], $(Ppy)^{[2]},$ $(PTh)^{[3]},$ polypyrrole polythiophene (o-phenylenediamine) (POPD)^[4], poly(1-naphthylamine) (PNA)[5] etc. have been extensively investigated for their potential application in the field of photocatalysis [6], fuel cells^[7], light emitting diodes^[8], biosensors^[9] and bioimaging[10-12]. Among these, PTh has received exceptional recognition due to its ease of processability and remarkable redox activity[13, 14]. Recently, graphene oxide (GO) has generated immense interest among researchers due to the emergence of new era of carbon-filled nanocomposites exhibiting superior mechanical, structural and thermal properties. GO is synthesized from low-cost graphite and serves as an attractive filler for the production of polymer nanocomposites. Nanocomposites based on conducting polymers with GO are widely reported due to their excellent synergistic properties and wide application in various devices^[15, 16].

It has been reported that GO and polyvinylpyrrolidone (PVP) composites revealed high electrocatalytic activity toward the reduction of O₂ and H₂O₂ and were proposed as

highly sensitive biosensor^[17]. GO has also been investigated to improve photovoltaic performance when incorporated with poly-3-hexathiophene (P3HT)^[18]. Hence, the advantage of GO over other organic-nanocarbon hybrids is that the composition can be altered to produce desirable optoelectronic properties. Lately, a reduced graphene oxide/polythiophene (RGO/Pth) aerogel was developed by Lu et al.[19] and it was established that the π - π effect between Pth and graphene resulted in uniform dispersion of Pth on graphene. Su et al. [20] designed polythiophene/reduced graphene oxide based on (Au, Ag or Pt) ternary nanocomposites for their application as ammonia gas sensors and Au/PTh/rGO ternary nanocomposite film had the highest response compared to other ternary nanocomposite films at room temperature. Mobin et al.[21] also developed ternary nanocomposites of polythiophene (PTh)-TiO₂-reduced graphene oxide (rGO) by chemical oxidative polymerization which were utilized for corrosion protective coatings.

Although there are many studies on bulk composites involving GO in the mixtures, scarce studies focus on the variation in the optoelectronic properties of CPs when

CONTACT Liju Yang Iyang@nccu.edu Department of Pharmaceutical Sciences, Biomanufacturing Research Institute and Technology Enterprise (BRITE), North Carolina Central University, Durham, North Carolina, USA; Ufana Riaz Ufana2002@yahoo.co.in Department of Chemistry and Biochemistry, North Carolina Central University, Durham, North Carolina, USA.

modified with GO for their potential application in photocatalysis. Due to the synergistic combination of the electro-activities of GO and PTh, the charge transfer from valence band (VB) to conduction band (CB) in the CP is expected to improve, and a reduction in the optical bandgap is anticipated as well. The present work therefore reports the modification of PTh with GO in different weight loadings, and were characterized using FTIR, UV-visible, X-ray diffraction and scanning electron microscopy (SEM) techniques. Their catalytic efficiency against the degradation of Alizarin yellow (AY), Basic Blue (BB) and Congo Red (CR) under sono-photocatalytic conditions were explored; and their antibacterial activity against *Bacillus subtilis* were also investigated under dark and light conditions.

2. Experimental

Thiophene (Fisher Scientific), anhydrous ferric chloride (FeCl₃) (Fisher Scientific), deionized water, n-hexane (n-C₆H₁₄) (Fisher Scientific), Alizarin Yellow (AY) (Fisher Scientific), Basic Blue (BB) (Fisher Scientific), and Congo Red (CR) (Fisher Scientific) were used as received.

2.1. Synthesis of PTh

Thiophene (0.4 ml) was dispersed in n-hexane in a 150 ml conical flask and stirred for 30 minutes on a magnetic stirrer at 20 °C. Anhydrous ferric chloride (2.4 g) was taken in a 100 ml beaker and dissolved in deionized water (20 ml) The ferric chloride solution was then added to the thiophene solution dropwise over a period of 30 min and stirred for 24 h at 20 °C. The mixture changed from a burnt orange color liquid to a thick dark brown precipitate. The precipitates were centrifuged and placed in the oven at 90 °C for 72 h.

2.2. Preparations of GO modified PTh

GO was prepared by Hummer's method as per reported studies^[22]. The nanohybrids of GO with PTh were formulated using 1 wt.%, 3 wt.% and 5 wt% of GO with PTh. The mixture was dispersed in deionized water and subjected to sonication for 2 h at 25 °C. The nanohybrids were then centrifuged and dried in an oven for 72 h to ensure the complete removal of water and were designated as 1-GO/PTh, 3-GO/PTh and 5-GO/PTh according to the loading of GO in the nanohybrid.

2.3. Sono-photocatalytic degradation studies

A 100-ppm stock solution of dyes Alizarin Yellow (AY), Basic Blue (BB), and Congo Red (CR)) was prepared and diluted to 50 ppm. Approximately 50 mg of the PTh and nanohybrid was added to 150 mL of 50 ppm solution and kept in darkness for ~1 h to establish equilibrium. The degradation was carried out on an ultrasonic bath under visible light for a period of 60 min. Aliquots of the degraded

sample were taken at 10 min interval and were centrifuged at a high speed (5000 rpm) using a centrifuge machine (REMI, Model R8C) to determine the concentration of degraded dye monitored using a UV-vis spectrophotometer model VWR, Model UV-3100PC.

2.4. Evaluation of antibacterial activity: Bacterial culture and cell preparation

Overnight freshly grown *B. subtilis* cells in Luria-Bertani (LB) broth were harvested by centrifugation and then washed twice with PBS. The cells were re-suspended in PBS, and further dilutions with desired cell concentrations were prepared for experimental uses. The actual cell concentrations in the samples were determined using the traditional surface plating method, in which the cell samples were 1/10 serial diluted in PBS, and aliquots of $100\,\mu\text{L}$ of appropriate dilutions were plated on LB agar plates. The colonies were counted after incubation at $37\,^{\circ}\text{C}$ for 18-24h, and calculated into colony forming unit (CFU) per mL for the cell concentration in each sample.

2.5. Minimum inhibitory concentration (MIC) assay

MIC is commonly used to evaluate the potency of an antimicrobial material in terms of the concentration at which it inhibits the growth of $\sim 1 \times 10^6$ challenge microorganisms during 18 - 20 h incubation period at 35 ± 2 °C. In this study, the MIC assay was performed using the standard 2-fold dilution method in a 96-well plate. Briefly, B. subtills cells prepared as above was diluted to the concentration of ~ 1×10^6 CFU/mL in LB broth. Aliquots of 135μ L/well B. subtills and 15 µL/well of the PTh or GO/PTh nanohybrids in 2-fold dilutions at concentrations ranging from 0.125 µg/ mL to 32 µg/mL were added to the wells. Samples of B. subtills cells with 15 µL/well 10% DMSO, or LB broth, as well as the samples without cells were used as various controls. All samples were duplicated. The plate was placed on an Orbital shaker (BT Lab Systems, St. Louis, MO) with shaking at 330 rpm for 1 h. The plate was then incubated at 37°C in the incubator for overnight (~24h). The optical density at 595 nm (OD595) values of the samples were measured before the treatment and after overnight incubation using the Max M5 spectrophotometer (Molecular Devices, LLC, Sunnyvale, CA). The changes in OD595 values were used to determine the growths of the cells. The MICs of the nanohybrids were the minimum concentration of the nanohybrids that showed no bacterial growth, e.g. no change in OD595, after 24h incubation compared to the OD measured before the treatment.

2.6. Disk diffusion inhibitory zone test

B. subtills cells were spread on a LB agar petri dish plate. Six blank disks were evenly distributed around the plate in 6 evenly divided sections onto the *B. subtills* plate. Aliquots of $20\,\mu\text{L}$ of each nanohybrid sample at the concentration of $50\,\mu\text{g/mL}$, and $20\,\mu\text{L}$ 10% DMSO as the control, were added

onto each disk. The plate was duplicated. Then, one plate with lid was exposed under the household daylight LED bulb by CREE (omnidirectional 815 lumens) placed at ~10 cm above the surface of the plate for 1 h, and the other duplicated plate was covered in aluminum foil as the dark control. After 1h treatment, the plates were incubated at 37°C overnight. The diameter of the inhibition zone around each disk was then measured and compared to indicate the inhibitory effect on the growth of Bacillus subtilis among the different samples.

2.7. Bactericidal dose response curves of nanohybrids

The nanohybrids samples were further assessed for their bactericidal effect on B. subtilis by examining the dose-dependent curves of each GO/PTh nanohybrids. B. subtilis samples containing ~106 to 107 CFU/mL were mixed with nanohybrid samples at 1:1 (v/v) in the wells of a 96-well plate with the final concentrations of the nanohybrids ranging from 0.5 to 6 µg/mL, with appropriate controls of samples without nanohybrids, all samples were prepared in duplicates. the plate was placed on the Orbital shaker with shaking at 330 rpm, with exposure to visible light from the LED bulb for 1h. After treatment, each sample was 1/10 serially diluted with PBS, appropriate dilutions were surface plated on LB agar plates. The colonies were counted after incubation at 37°C for 18-24h, and calculated into colony forming unit (CFU) per mL for the viable cell number in each sample. The viable cells reduction for a given sample was calculated as the difference between the logarithmic viable cell number of the control and that of the sample at a given concentration.

2.8. Scanning electron microscopic (SEM) imaging of nanohybrids-treated cells

SEM imaging of nanohybrids-treated cells were performed at the Microscopy Services Laboratory, Department of Pathology and Laboratory Medicine, at University of North Carolina at Chapel Hill (UNC-CH). To prepare the treated bacterial samples for SEM imaging, B. subtilis cells in exponential stage were collected, washed with PBS, and resuspended in PBS (at OD595nm~0.42). Equal volume of B. subtilis cells and 2 µg/mL nanohybrids in 10% DMSO were added to duplicate wells of a 6-well plate with a total volume of 3 mL/ well and the final concentration of nanohybrids at 1 µg/mL. The plate was placed on the Orbital shaker with shaking at 330 rpm and exposed under a commercial 8W daylight LED lamp (CREE, omnidirectional 815 lumens) for 1h. After the treatment, the duplicate samples were collected, centrifuged at 9000 rpm (12,156 x g) for 2 min and 5000 rpm (3,752 x g) for 5 min to pellet the cells (Beckman Coulter Avanti J-26 XP centrifuge with the JLA 16.250 rotor), followed by washing with PBS. Then, the sample was transferred to a 1.5 mL centrifuge tube, followed by centrifugation (the Eppendorf 5424 microcentrifuge) at 1000 rpm (94 x g) for 10 min to concentrate the cell into a pellet, removal of supernatant, and adding 1 mL fixative solution of 2.5% glutaraldehyde in

0.1 sodium cacodylate, pH7.4. The fixed samples were stored in refrigerator overnight or until further use for imaging.

The fixed bacterial samples were plated on 12 mm round glass coverslips and allowed to adhere at 4°C overnight. Coverslips were washed three times with 0.15M sodium phosphate buffer then incubated with 1% buffered osmium tetroxide for 30 minutes at room temperature. Coverslips were then washed three times in deionized water and dehydrated through an ascending series of ethanol (30%, 50%, 75%, 100%, 100% 100%). Coverslips were transferred in 100% ethanol to a Samdri-795 critical point dryer and dried using liquid carbon dioxide as the transitional solvent (Tousimis Research Corporation, Rockville, MD). Once dry, coverslips were mounted on 13 mm diameter aluminum stubs using carbon adhesive tabs and sputter coated with 5 nm of a 60:40 gold/palladium alloy using a Cressington 208HR Sputter Coater (Ted Pella Inc, Redding CA). Images were obtained using a Zeiss Supra 25 FESEM operating at 5kV using an SE2 detector, 20 µm aperture, and approximate working distances of 5 to 8 mm (Carl Zeiss Microscopy, LLC, Peabody, MA).

3. Characterization

3.1. Spectral studies

FT-IR spectra of PTh and GO were taken on the FT-IR spectrophotometer (Agilent Cary 630), in the solid form. Ultraviolet-visible light (UV-vis) spectra we're taken on an UV-vis spectrophotometer (VWR, Model UV-3100PC) using the dyes as the solvent. The peak parameters were analyzed using a UV-vis analyst software.

3.2. XRD studies

XRD patterns of the nanocomposites were recorded on a powder diffractometer (Philips, Model PW 3710) (using a Ni filtered Cu Kα radiation). Peak parameters were analyzed using Origin 6.1 software.

3.3. SEM-EDS analysis

SEM micrographs (TEM) were obtained using a Morgagni Model 268-D (FEI, USA).

3.4. XPS studies

X-ray photoelectron spectroscopy (XPS) spectra were collected using a Physical Electronics Versa Probe II instrument equipped with a monochromatic Al Ka X-ray source ($hv = 1,486.7 \, eV$) and a concentric hemispherical analyzer. Charge neutralization was performed using both low energy electrons (<5 eV) and argon ions.

4. Results and discussion

4.1. IR analysis

The IR spectrum of PTh (given in supporting information as Figure S1(a-d)) exhibited peak at 3230 cm⁻¹ due to the

presence of entrapped water. The peaks at 1806 cm⁻¹ and 1675 cm⁻¹ was attributed to the C=C stretching vibration of conjugated alkenes group present in PTh. The peak at 1353 cm⁻¹ was attributed to the C-H bending vibration in PTh, whereas the peaks at 1172 cm⁻¹ was assigned to the C-S-C stretching vibrations^[23, 24]. The addition of GO revealed a major reduction in the peak intensities of $1675\,\mathrm{cm^{-1}}$ and $1172\,\mathrm{cm^{-1}}$ suggesting intense interaction between the O of GO and the C=C of PTh. The reduction in the intensities of these peaks was found to be more pronounced with the increase in the loading of GO that confirmed synergistic interaction between PTh and GO.

4.2. UV analysis

The UV-visible spectrum of pure PTh, Figure 1, showed peaks at 400 nm related to $n-\pi^*$ transition. Upon modification with 1 wt.% GO, a shift in the peak position of PTh was noticed from 400 nm to 425 nm^[23]. The UV spectrum of 3-GO/PTh revealed peaks at 340 nm and 465 nm. The peak at 350 nm was related to the presence of GO in the nanohybrid. Similarly, 5-GO/PTh revealed intense peaks at 350 nm and 465 nm due to the presence of higher concentration of GO in PTh.

The PTh polaronic peak was notice to shift to 465 nm upon modification with GO. Interestingly, the electronic transitions were found to show a major change upon modification with GO suggesting the overlap of the orbitals between GO and PTh and the formation of nanohybrid. The band gap was computed to be 2.63 eV for PTh, 2.54 eV for 1-GO/PTh, 2.3 eV for 3-GO/PTh and 2.1 eV for 5-GO/PTh.

4.3. SEM-EDS analysis

The SEM of PTh, Figure 2(a), exhibited a fine fibrous morphology, in which the particles were deeply embedded in one another and formed a porous structure. The SEM image of 1-GO/PTh, Figure 2(b), showed granular morphology

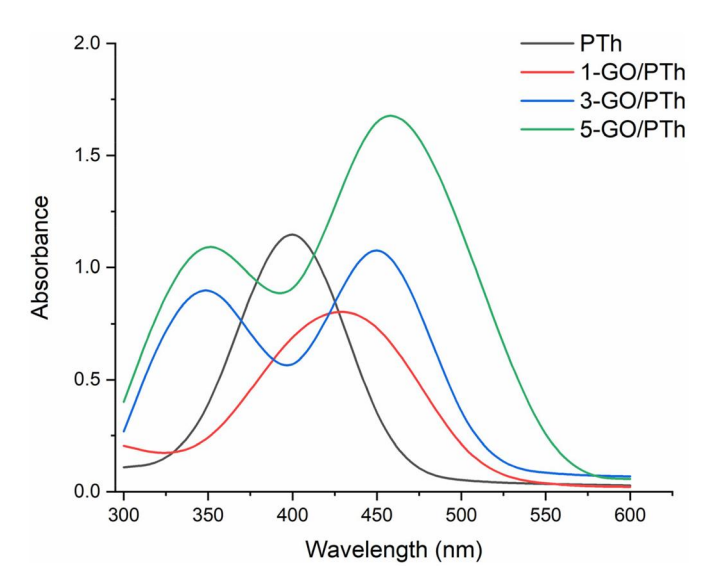


Figure 1. UV-visible spectra of PTh and GO/PTh nanohybrids.

with intense bright clusters formed at the surface. The SEM image of 3-GO/PTh, Figure 1(c), revealed an increase in the size of the granular clusters upon increase in the loading of GO in PTh. Similarly, 5-GO/PTh, Figure 1(d), exhibited formation of a flaky morphology with granular agglomerates.

The SEM studies clearly reflected the variation in the morphology upon loading of GO in the nanohybrid. The EDS spectra of PTh and GO modified PTh (given in supporting information as Figures S2(a-d) and S3(a-e)), confirmed the elemental composition of PTh and its doping with Cl ions via the initiator (FeCl₃) used in polymerization. The existence of O on the surface of PTh in GO modified PTh confirmed the encapsulation of PTh by GO.

4.4. XRD analysis

The XRD of PTh, (given in supporting information as Figure S4) revealed peaks at $2\theta = 32^{\circ}$, 33° , 34.5° 38° and 46° with maximum intensity observed at $2\theta = 32^{\circ}$. The presence of sharp and intense peaks revealed a highly ordered and crystalline structure of PTh[23, 24]. The peaks showed no changes upon modification with GO suggesting encapsulation of the polymer with GO.

4.5. XPS analysis

To gain a better understanding of the interactions between PTh and GO we measured the XPS spectrum as shown in Figure 3(a-e) Apart from the presence of C 1s and O 1s signals, in PTh, Figure 3(a) typical S 2s, and Cl 2p peaks can be observed as well, indicating the PTh had been doped with the chloride ions. The XPS survey spectrum of 5-GP/ PTh, Figure 3(b), showed peaks corresponding to O 1s indicating the presence of GO. The Figure 3(c) shows the high-resolution C 1s signal can be deconvoluted to give six peaks at 282.29 eV, 282.62 eV, 283.6 eV, 286.5 eV, 287.1 eV and 287.16 eV, corresponding to carbon atoms in different functional groups, C=C, C=O, C-S and C-C. The high-resolution spectrum of C 1s for 5-GO/PTh, Figure 3(d), showed deconvoluted peaks at 281.8 eV, 282.4 eV, 283.7 eV, 283.76 eV, 286.81 eV and 286.88 eV, corresponding to carbon atoms of C=C, C=O, C-S and C-C. In the O 1s spectrum, peaks were noticed at 527.64 eV, 528.27 eV, 529 eV, 533.13 eV, 532.76 eV, 533.61 eV and 536.65 eV, which were attributed to S=O, S-O/C-O and C-O-C=O respectively^[25, 26]. The peaks confirmed the interaction of GO with PTh.

4.6. Sono-photocatalytic degradation studies

Degradation of AY, BB and CR dyes was performed via sonication under visible light for a period of 60 min (given in supporting information as Figures S5, S6 and S7(a-d)). In presence of 50 mg of pristine PTh, 20 % degradation of AY was noticed, while BB and CR dyes showed 30% and 40 % degradation respectively, Figures 4(a-c) and 5. In presence of 1-GO/PTh, the degradation was increased to 45% for AY, 40% for BB and 60% for CR. However, using 3-GO/PTh, the degradation was increased to 70% for AY, 65% for BB and

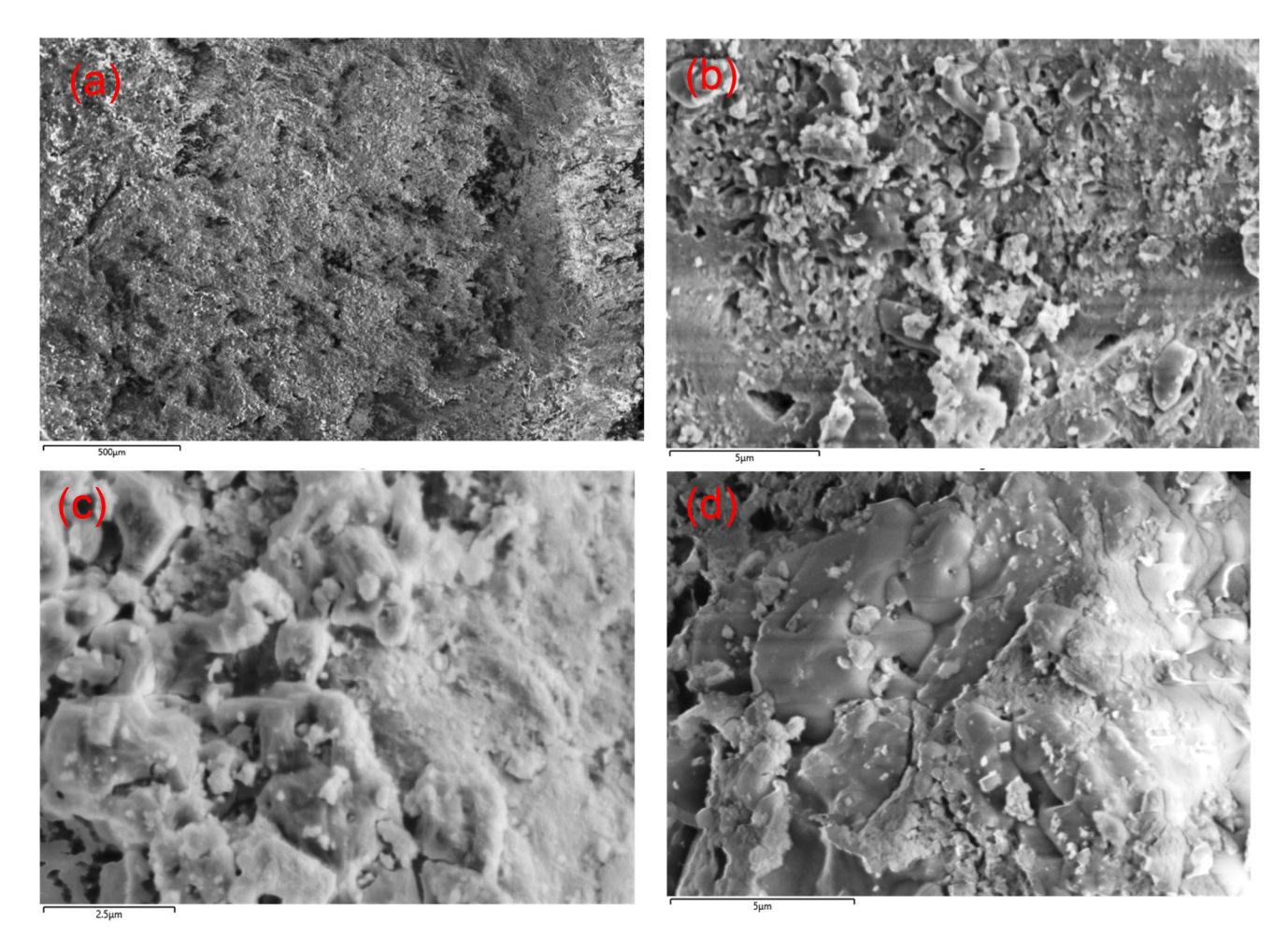


Figure 2. SEM Of (a) PTh, (b) 1-GO/PTh, (c) 3-GO/PTh, (d) 5-GO/PTh.

72% for CR while using 5-GO/PTh, the degradation for AY was noticed to be 80%, for BB it was noticed to be 85% while for CR, it was computed to be 95%. The degradation was noticed to increase with increase in the loading of GO in the nanohybrids.

4.7. Disk diffusion inhibitory effect with and without light exposure

The disk inhibition test using 20 µL of 50 µg/mL each GO/ PTh, and PTh, in 10% DMSO showed that all the GO/PTh nanohybrids and PTh exhibited significant inhibitory effect on the growth of B. subtilis cells (Figure 6). Among the GO/PTh nanohybrids, the 3% GO/PTh nanohybrids showed the most effective inhibition but was similar to that of PTh without GO doping, followed by the 1% GO/PTh and 5% GO/PTh which showed similar inhibitory effects (Figure 6). It is noted that the inhibitory effects by these nanohybrids were the same with and without light exposure, indicating there is no photoactivation needed for the nanohybrids or PTh to exhibit their antibacterial effects. Also interesting is the doping of GO in PTh did not enhance the antibacterial activity, rather reduced its antibacterial activity by 1% and 5% doping, but 3% doping of GO kept its antibacterial activity the same as non-doped PTh. The data clearly shows that the antibacterial activity

is due to the presence of PTh and GO. However, the activity shown by 3% GO/PTh may be presumably due to the differences in the encapsulation of PTh by GO. The SEM of 3% GO/PTh shows that the surface has higher PTh particles and GO seems to be embedded within PTh. Therefore, this hybrid shows higher antibacterial activity as compared to the other nanohybrids as they have GO to be present on the surface which prevent PTh from interacting with the bacteria. Hence, it can be concluded that the morphology of PTh, its encapsulation with GO and the surface structure of the nanohybrids are the factors that govern the antibacterial activity.

4.7. MIC and bactericidal dose-dependent curves of the nanohybrids

The MIC assay was used to evaluate the potency of these nanohybrids in terms of the minimal concentration at which it inhibits the growth of $\sim 1 \times 10^6$ B. subtilis. The standard 2-fold micro dilution method was used to test the nanohybrids in the concentration range of 0.125 μg/mL to 32 μg/mL of each sample to determine the MICs. The results of MIC assay indicated that PTh and 3% GO/PTh had a MIC of 2 μg/mL, while 1% and 5% GO/PTh had a MIC of 4 μg/mL, which were consistent with the order of the inhibitory effects obtained in the disk diffusion inhibitory test.

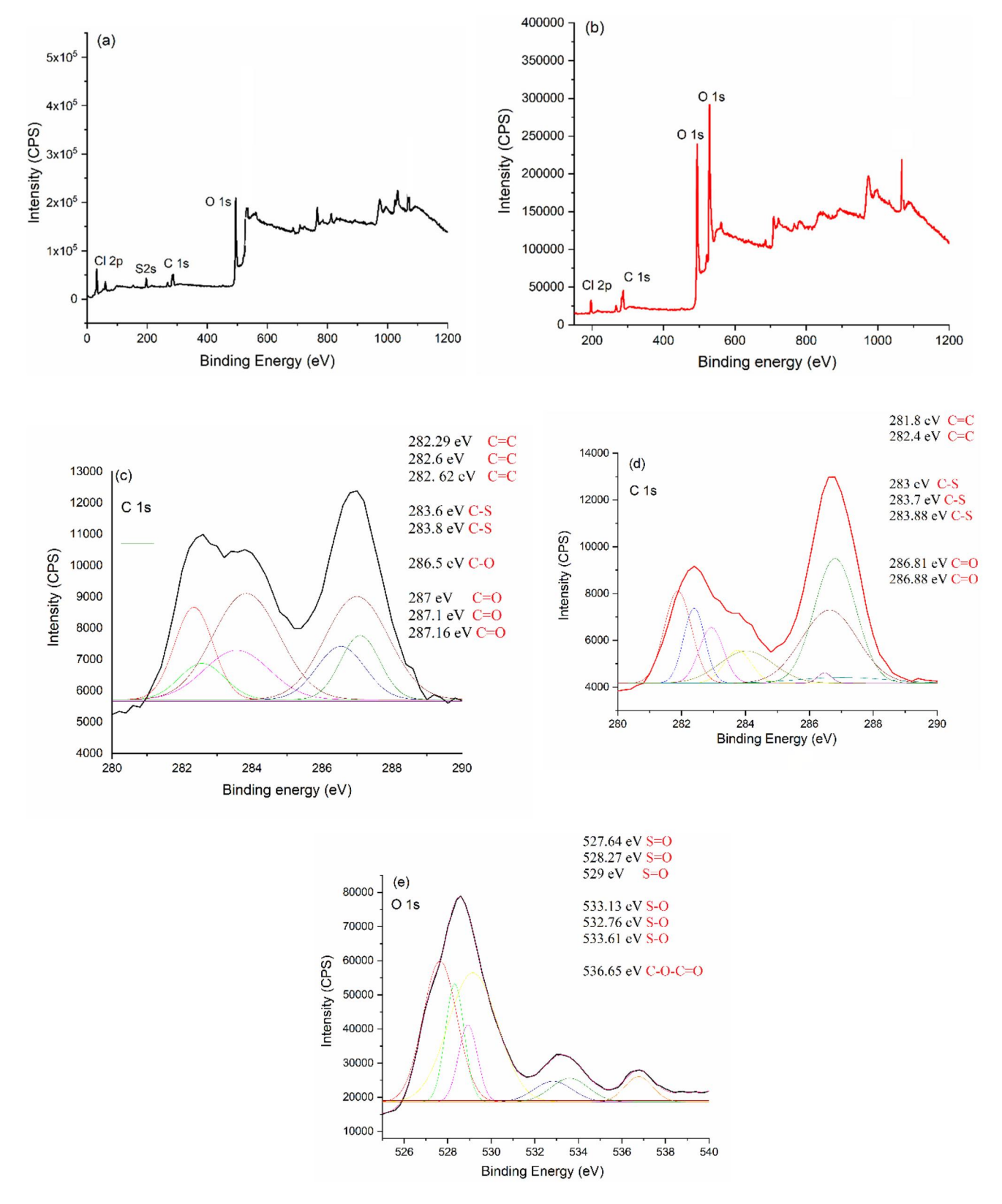


Figure 3. (a) XPS survey spectrum of PTh, (b) XPS survey spectrum of 5-GO/PTh (c) high resolution C 1s of PTh, (d) high resolution C 1s of 5-GO/PTh, (e) high resolution O 1s of 5-GO/PTh.

Further, we examined the bactericidal effect of these nanohybrids against *B. subtilis* with 1h treatment time by examining the dose-dependent curves of each GO/PTh nanohybrids in the concentration range of 0.5 to $4 \mu g/mL$ (Figure 7a). As shown in the figure, upon 1h treatment to

the *B. subtilis* samples containing $\sim 10^6$ to 10^7 CFU/mL, 3%GO/PTh and PTh showed a very sharp reduction of viable cell number upon the treatment, and completely killed all the cells in the samples by $1\,\mu\text{g/mL}$. However, 1% and 5% GO/PTh showed a much slower rate of killing

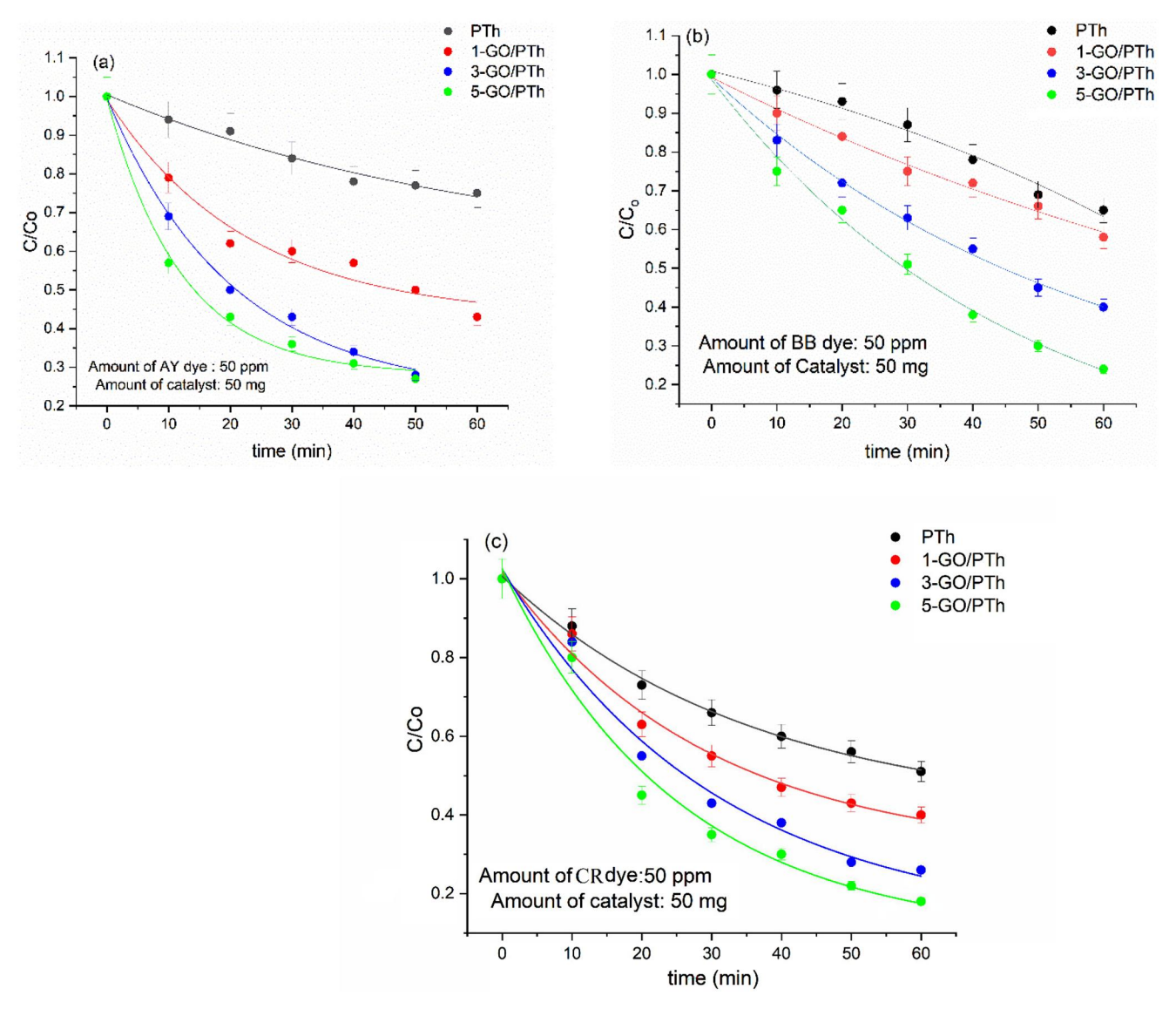


Figure 4. C/Co Plots for degradation of dyes in presence of (a)AY dye, (b) BB dye and (c) CR dye using PTh and GO/PTh nanohybrids.

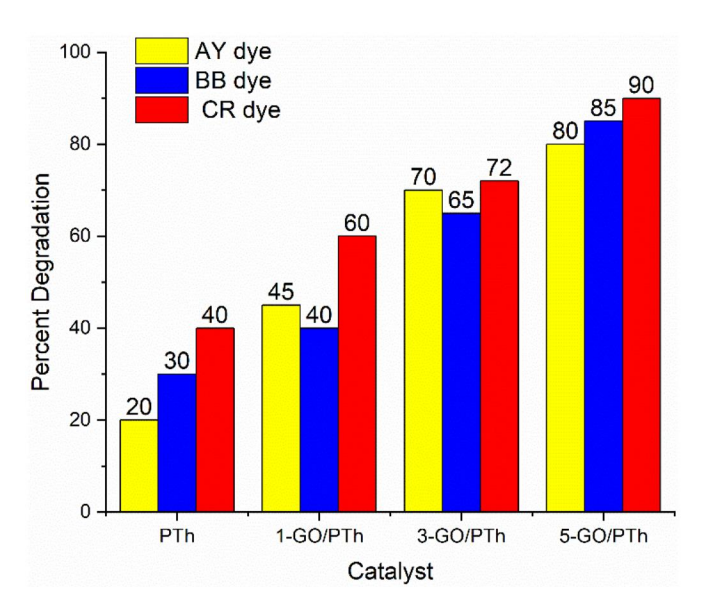


Figure 5. Percent degradation of dyes in presence of PTh and GO/PTh nanohybrids.

the cells, and needed higher concentration up to 3 and 4μg/mL to completely kill the cells in the samples, respectively. Again, the relative bactericidal efficiencies of the PTh and GO/PTh nanohybrids showed in the dosedependent manner were generally consistent with the above MIC and the disk diffusion inhibitory test. Figure 7b and 7c show the representative images of control B. subtilis cells and the cells after PTh treatment, which confirmed the damaged and dead cells in the treated samples. In summary, the results from multiple tests on the antibacterial function of PTh and GO/PTh nanohybrids consistently indicated that PTh has excellent antibacterial function with or with light activation, the GO/PTh nanohybrids also have considerably effective antibacterial function, however, the doping of GO is not necessarily to improve the antibacterial function, on the contrast, inappropriate ratio of GO doping may reduce the antibacterial activity. The observation suggests that the antibacterial mechanisms of PTh and GO/PTh might be different from their photocatalytic activity to degrade dyes.

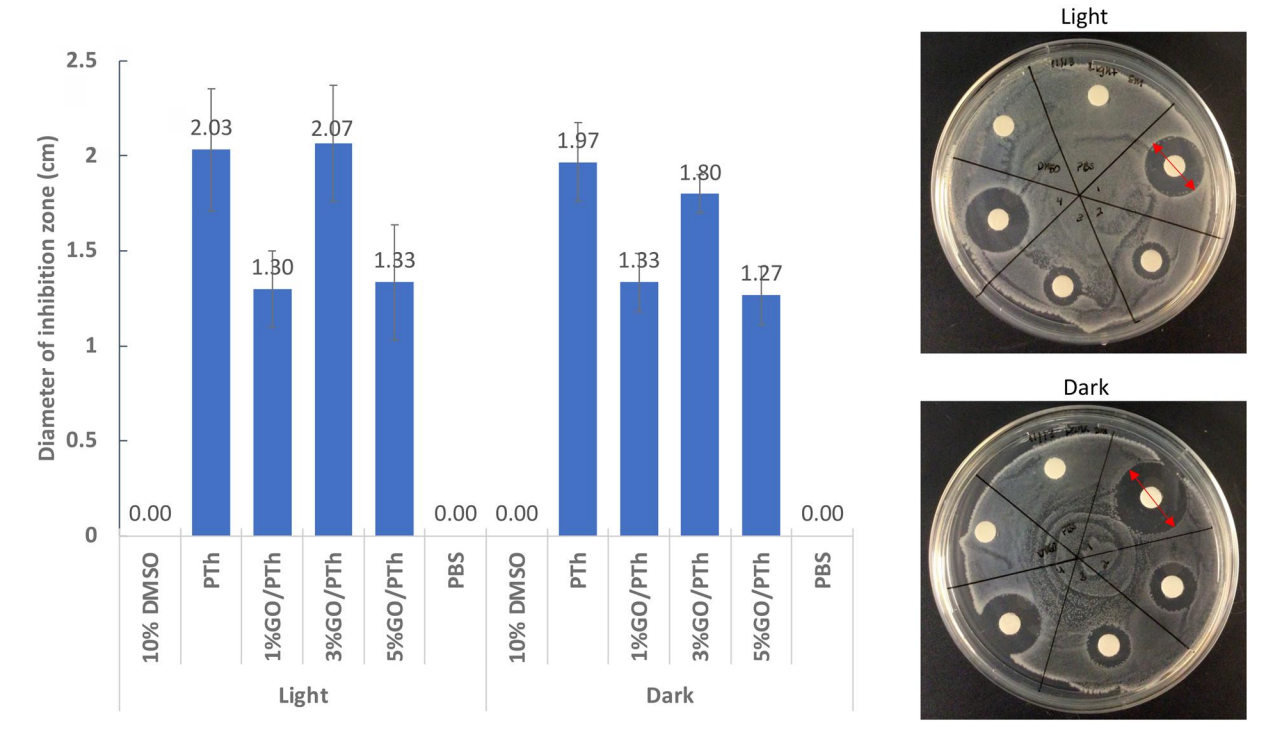


Figure 6. The diameters of inhibition zones by the GO/PTh nanohybrids and PTh, with and without 1h visible light exposure, to the growth of *B. subtilis* cells on LB agar. Aliquot of 20 μL of each GO/PTh, and PTh, at 50 μg/mL in 10% DMSO was placed on each disk, 10% DMSO and PBS were used as the control. Sample no on the plates: 1: 3%GO/PTh; 2: 5% GO/PTh; 3: 1% GO/PTh; 4: PTh; 10% DMSO, and PBS. The red arrow line on the plate show how the diameter of an inhibition zone was measured. The data on the column shows the averaged measurement of the inhibition zone by the given nanohybrids or control reagent.

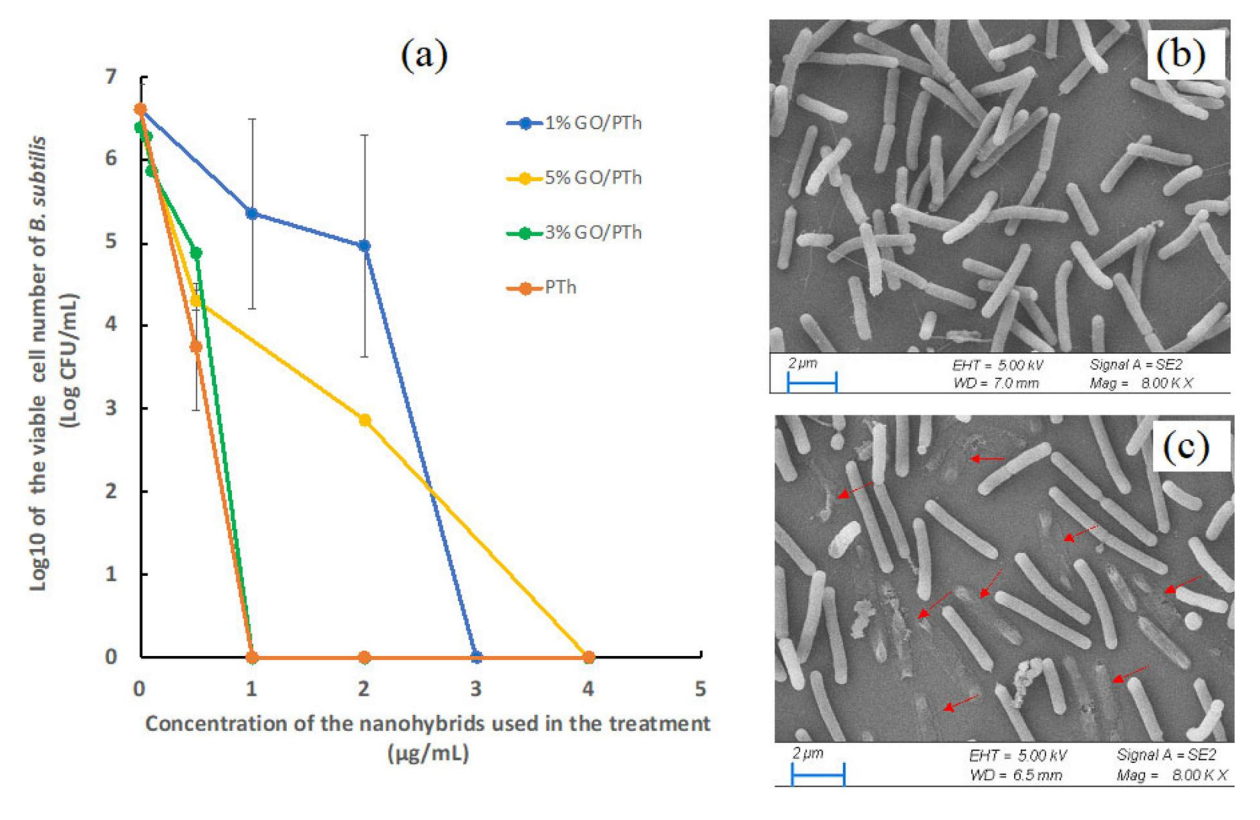


Figure 7. (a) The bactericidal dose-dependent curves of PTh and GO/PTh nanohybrids against *B. subtilis* cells, with 1h treatment time; (b) Representative SEM image of untreated *B. subtilis* cells; and (c) Representative SEM image of *B. subtilis* cells after PTh treatment. Red arrows indicate examples of the dead cells after PTh treatment.



5. Conclusion

Photocatalytic degradation of Alizarin, Yellow, Congo Red and Basic Blue dyes was carried out using PTh and graphene oxide modified PTh. The dyes showed the highest degradation using 5-GO/PTh as a photocatalyst. The methodology adopted in this study demonstrates the efficiency of GO in sensitizing PTh for rapid degradation of pollutants. Future research is needed for the development of more efficient catalysts, which are of low cost and can be regenerated easily. The mechanism of degradation and catalyst regeneration studies are under investigation in our laboratory and will be published soon. On the antibacterial function, the results from the disk diffusion test, the MIC test, and the bactericidal effect test, are consistently indicated that PTh itself exhibited highly effective antibacterial function, light activation is not necessary. The doping of GO did not enhance the antibacterial function of the nanohybrids, rather the high and low doping of GO (1% or 5%) could reduce the antibacterial function.

Acknowledgements

The Microscopy Services Laboratory, Department of Pathology and Laboratory Medicine at UNC-CH, is supported in part by P30 CA016086 Cancer Center Core Support Grant to the UNC Lineberger Comprehensive Cancer Center. The authors wish to acknowledge National Science Foundation (Award # 2122044), the NSF PREM for Hybrid Nanoscale Systems between NCCU and Penn State for providing financial assistance. The authors also wish to thank Rowan Katzbaer for acquiring the XPS and the SEM data.

Disclosure statement

The authors declare no conflict of interest

References

- [1] Ekande, O. S.; Kumar, M. Review on Polyaniline as Reductive Photocatalyst for the Construction of the Visible Light Active Heterojunction for the Generation of Reactive Oxygen Species. J. Environ. Chem. Eng. 2021, 9, 105725. DOI: 10.1016/j. jece.2021.105725.
- [2] Chouli, Y.; Mokhtari, F. B.; Zeid, S. A.; Dragoe, D.; Martin, R. S.; Brisset, F.; Remita, H.; Remita, S. Superior Photocatalytic Activity of Polypyrrole Nanostructures Prepared by Radiolysis in Water and Dichloromethane. Rad. Chem. Phy. 2022, 195, 110079. DOI: 10.1016/j.radphyschem.2022.110079.
- [3] Zia, J.; Fatima, F.; Riaz, U. A Comprehensive Review on the Photocatalytic Activity of Polythiophene-Based Nanocomposites against Degradation of Organic Pollutants. Catal. Sci. Technol. 2021, 11, 6630-6648. DOI: 10.1039/D1CY01129D.
- [4] Zia, J.; P, M.; Riaz, U. Photocatalytic Degradation of anti-Inflammatory Drug Using POPD/Sb2O3 Organic-Inorganic Nanohybrid under Solar Light. J. Mater. Res. Technol. 2019, 8, 4079-4093. DOI: 10.1016/j.jmrt.2019.07.017.
- Jadoun, S.; Verma, A.; Ashraf, S. M.; Riaz, U. A Short Review on the Synthesis, Characterization, and Application Studies of Poly(1-Naphthylamine): A Seldom Explored Polyaniline Derivative. Colloid Polym Sci. 2017, 295, 1443-1453. DOI: 10.1007/s00396-017-4129-2.
- [6] Kumar, R.; Sejdic, J. T.; Padhye, L. P. Conducting Polymers-Based Photocatalysis for Treatment of Organic Contaminants in Water.

- Chem. Engg. J. Adv. 2020, 4, 100047. DOI: 10.1016/j. ceja.2020.100047.
- Ghosh, S.; Das, S.; Mosquera, M. E. G. Conducting Polymer-Based Nanohybrids for Fuel Cell Application. Polymers (Basel) 2020, 12, 2993. DOI: 10.3390/polym12122993.
- Wang, Z.; Wu, Z.; Weng, L.; Ge, S.; Jiang, D.; Huang, M.; Mulvihill, D. l M.; Chen, Q.; Guo, Z.; Jazzar, A.; et al. A Roadmap Review of Thermally Conductive Polymer Composites: Critical Factors, Progress, and Prospects. Adv. Funct. Mater. 2023, 33, 2301549. DOI: 10.1002/adfm.202301549.
- [9] Keirouz, A.; Mustafa, Y. L.; Turner, J. G.; Lav, E.; Jungwirth, U.; Marken, F.; Leese, H. S. Conductive Polymer-Coated 3D Printed Microneedles: Biocompatible Platforms for Minimally Invasive Biosensing Interfaces. Small 2023, 19, e2206301. DOI: 10.1002/ smll.202206301.
- Sharma, A. K. Current Trends in Nanotheranostics: A Concise Review on Bioimaging and Smart Wearable Technology. Nanotheranostics 2023, 7, 258-269. DOI: 10.7150/ntno.82886.
- [11] Šeděnková, I.; Taboubi, O.; Paúrová, M.; Hromádková, J.; Babič, M. Influence of the Type and Concentration of Oxidant on the Photoacoustic Response of Polypyrrole Nanoparticles for Potential Bioimaging Applications. Synth. Met. 2023, 292, 117218. DOI: 10.1016/j.synthmet.2022.117218.
- [12] Lee, K.-W.; Wan, Y.; Huang, Z.; Zhao, Q.; Li, S.; Lee, C.-S. Organic Optoelectronic Materials: A Rising Star of Bioimaging and Phototherapy. 2023 (accepted).
- [13] Hassan, A.; Ismail, M.; Reshak, A. H.; Zada, Z.; Khan, A. A.; M, F. U. R.; Arif, M.; Siraj, K.; Zada, S.; Murtaza, G.; Ramli, M. M. Effect of Heteroatoms on Structural, Electronic and Spectroscopic Properties of Polyfuran, Polythiophene and Polypyrrole: A Hybrid DFT Approach. J. Mol. Struc. 2023, 1274, 134484. DOI: 10.1016/j. molstruc.2022.134484.
- [14] Guo, Q.; Du, C.; Deng, X.; Cheng, Y.; Tai, X.; Nie, G. High Performance Polythiophene Derivative with Good Electrochromic and Energy Storage Properties Electrochemical Synthesized in Boron Trifluoride Diethyl Etherate. Dyes. Pigm. 2023, 220, 111709. DOI: 10.1016/j.dyepig.2023.111709.
- [15] Ates, M.; Alperen, C. Polythiophene-Based Reduced Graphene Oxide and Carbon Black Nanocomposites for Supercapacitors. Iran Polym. J. 2023, 32, 1241-1255. DOI: 10.1007/s13726-023-01201-9.
- [16] Shindalkar, S. S.; Reddy, M.; Singh, R.; Nainar, M. A. M.; Kandasubramanian, B. Polythiophene Blends and Composites as Potential Energy Storage Materials. Synth. Met. 2023, 299, 117467. DOI: 10.1016/j.synthmet.2023.117467.
- Lawal, A. T. Recent Developments in Electrochemical Sensors Based on Graphene for Bioanalytical Applications. Sens. Biores. 2023, 41, 100571. DOI: 10.1016/j.sbsr.2023.100571.
- [18] Zheng, F.; Yang, X.-Y.; Bi, P.-Q.; Niu, M.-S.; Lv, C.-K.; Feng, L.; Qin, W.; Wang, Y.-Z.; Hao, X. T.; Ghiggino, K. P. Poly(3-Hexylthiophene) Coated Graphene Oxide for Improved Performance of Bulk Heterojunction Polymer Solar Cells. Org. Electron. 2017, 44, 149-158. DOI: 10.1016/j.orgel.2017.02.021.
- [19] Lu, Y.; Gao, Z.; Yang, Q.; Xiong, C.; Hu, G.-H. 3.6 V High-Voltage Symmetrical Supercapacitor Based on Reduced Graphene Oxide/ Polythiophene Aerogels with Uniform Dispersion. J. Energy. Storage 2023, 72, 108224. DOI: 10.1016/j.est.2023.108224.
- [20] Su, P.-G.; Tsai, M.-S.; Lu, C.-J. Fabrication of Noble Metal (Au, Ag, Pt)/Polythiophene/Reduced Graphene Oxide Ternary Nanocomposites for NH3 Gas Sensing at Room Temperature. Anal. Met. 2022, 14, 4113-4121. DOI: 10.1039/d2ay01317g.
- [21] Mobin, M.; Ansar, F. Polythiophene (PTh)-TiO2-Reduced Graphene Oxide (rGO) Nanocomposite Coating: Synthesis, Characterization, and Corrosion Protection Performance on Low-Carbon Steel in 3.5 wt % NaCl Solution. ACS Omega 2022, 7, 46717-46730. DOI: 10.1021/acsomega.2c05678.
- [22] Yoo, M. J.; Park, H. B. Effect of Hydrogen Peroxide on Properties of Graphene Oxide in Hummers Method. Carbon 2019, 141, 515-522. DOI: 10.1016/j.carbon.2018.10.009.
- [23] Riaz, U.; Farooq, A.; Alam, J. Microwave-Assisted Rapid Degradation of Methyl Red Dye Using Polyfuran/Polythiophene

- - and Its Co-Oligomers as Catalysts. Spectrochim. Acta A Mol. Biomol. Spectrosc. 2023, 302, 123106. DOI: 10.1016/j.saa.2023.123106.
- [24] Riaz, U.; Gaffar, S.; Hauser, K.; Yan, F. Visible-Light Induced Degradation of Diphenyl Urea and Polyethylene Using Polythiophene Decorated CuFe₂O₄ Nanohybrids. Nat. Sci. Rep. 2023, 13, 4975.
- [25] Alam, K.; Sim, Y.; Yu, J.; Gnanaprakashan, J.; Choi, H.; Chae, Y.; Sim, U.; Cho, H.; Cho, H. In-Situ Deposition of Graphene Oxide
- Catalyst for Efficient Photoelectrochemical Hydrogen Evolution Reaction Using Atmospheric Plasma. Materials 2019, 13, 12. DOI: 10.3390/ma13010012.
- [26] Li, Y.; Zhou, M.; Wang, Y.; Pan, Q.; Gong, Q.; Xia, Z.; Li, Y. Remarkably Enhanced Performances of Novel Polythiophene-Grafting-Graphene Oxide Composite via Long Alkoxy Linkage for Supercapacitor Application. Carbon 2019, 147, 519-531. DOI: 10.1016/j.carbon.2019.03.030.